THE JOURNAL OF PHYSICAL CHEMISTRY A

Article

pubs.acs.org/JPCA

OH-Initiated Heterogeneous Aging of Highly Oxidized Organic Aerosol

Sean H. Kessler,[†] Theodora Nah,[‡,§] Kelly E. Daumit,[∥] Jared D. Smith,[‡] Stephen R. Leone,[§] Charles E. Kolb,[⊥] Douglas R. Worsnop,[⊥] Kevin R. Wilson,[‡] and Jesse H. Kroll*[,†,∥]

[†]Department of Chemical Engineering, Massachusetts Institute of Technology, Cambridge Massachusetts 02139, United States

[‡]Chemical Sciences Division, Lawrence Berkeley National Laboratory, Berkeley California 94720, United States

[§]Department of Chemistry, University of California, Berkeley, California 94720, United States

[∥]Department of Civil and Environmental Engineering, Massachusetts Institute of Technology, Cambridge, Massachusetts 02139, United States

[⊥]Center for Aerosol and Cloud Chemistry, Aerodyne Research Inc., Billerica, Massachusetts 01821, United States

ABSTRACT: The oxidative evolution ("aging") of organic species in the atmosphere is thought to have a major influence on the composition and properties of organic particulate matter but remains poorly understood, particularly for the most oxidized fraction of the aerosol. Here we measure the kinetics and products of the heterogeneous oxidation of highly oxidized organic aerosol, with an aim of better constraining such atmospheric aging processes. Submicrometer particles composed of model oxidized organics—1,2,3,4-butanetetracarboxylic acid ($C_8H_{10}O_8$), citric acid ($C_6H_8O_7$), tartaric acid ($C_4H_6O_6$), and Suwannee River fulvic acid—were oxidized by gas-phase OH in a flow reactor, and the masses and elemental composition of the particles were monitored as a function of OH exposure. In contrast to our previous studies of less-oxidized model systems (squalane, erythritol, and levoglucosan), particle mass did not decrease significantly with heterogeneous oxidation. Carbon content of the aerosol always decreased somewhat, but this mass loss was approximately balanced by an increase in oxygen content. The estimated reactive uptake coefficients of the reactions range from 0.37 to 0.51 and indicate that such transformations occur at rates corresponding to 1−2 weeks in the atmosphere, suggesting their importance in the atmospheric lifecycle of organic particulate matter.

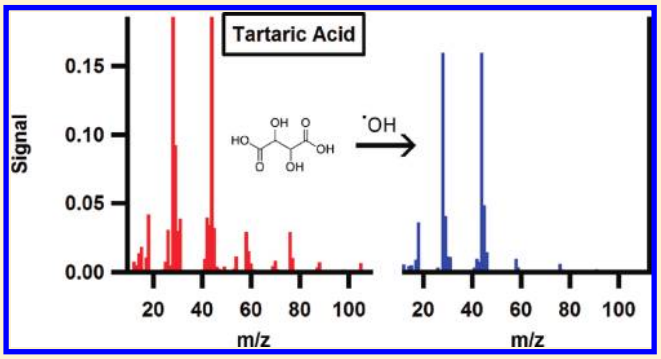

INTRODUCTION

A major uncertainty in the prediction of the climate and health effects of fine atmospheric particulate matter is the extent to which organic particles may undergo physical and/or chemical changes over their atmospheric lifetimes.[1] Organic aerosol can contain a significant fraction of reduced carbon and so is expected to undergo oxidation in the atmosphere; however, the rates, products, and effects on aerosol properties of such oxidation (aging) reactions are not well constrained. Detailed studies of such effects have been impaired by the difficulty of reproducing the atmospheric formation of highly oxidized aerosol in the laboratory.[2−4] Additionally, the sheer chemical complexity of organic mixtures, which can consist of several thousands or millions of compounds,[5] further impedes exact chemical characterization of the evolving organic aerosol.

To better understand key features of the chemistry of organic aerosol, several recent studies have focused on one class of aging reactions, the heterogeneous oxidation of organic particles by gas-phase hydroxyl radicals (OH).[2,6−12] These studies have typically examined the oxidation of model single-component systems, which serve as rough surrogates for varying classifications and levels of oxidation of organic particles. For example, our previous studies examined the oxidation of squalane ($C_{30}H_{62}$, a surrogate for primary, hydrocarbon-like organic aerosol),[10,11] erythritol ($C_4H_{10}O_4$, a tracer for isoprene-derived secondary organic aerosol),[12] and levoglucosan ($C_6H_{10}O_5$, a key component of aerosol from biomass burning).[12] This work indicated that as particles are progressively aged, the degree of oxidation of the particulate carbon increases. Moreover, volatilization processes become increasingly dominant at these higher levels of oxidation, leading to significant decreases in aerosol loading.[10,12]

Our previous work, and similar studies by other groups,[2,8,10−13] focused on the oxidation of relatively reduced organic aerosol, with average carbon oxidation states[5] of 0 or lower. Ambient measurements have shown that a large fraction of atmospheric organic aerosol is substantially more oxidized

Special Issue: A. R. Ravishankara Festschrift

Received: December 15, 2011
Revised: March 13, 2012
Published: April 6, 2012

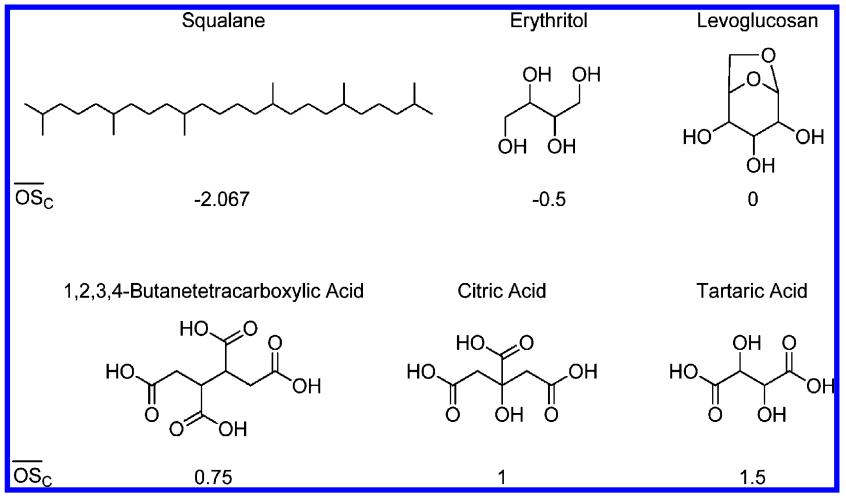

Figure 1. Molecular structure and average carbon oxidation state of the compounds used in previous studies (first row), and of the oxidized acids used in the single-component experiments in this study (second row). Fulvic acid does not have a single defined structure and so is not pictured.

than this, with average carbon oxidation states as high as +1.[1,5] However, the reactivity (oxidation kinetics and products) of this oxidized organic aerosol is almost completely unconstrained at present; this limits our ability to accurately model the evolution and fate of atmospheric organic aerosol. The goal of this work is thus to study the oxidative aging chemistry of this already highly oxidized aerosol in the laboratory. Because of the very low volatility of the constituent organics,[14−16] the fraction present in the gas phase is expected to be negligible, so that their oxidation must necessarily occur in the condensed phase. Therefore, the aging mechanism probed in these experiments—heterogeneous oxidation by OH—is likely to be important in the atmospheric evolution of this class of organic aerosol.

METHODS

As in our previous studies of less-oxidized species, the aging kinetics and chemistry of the aerosol are probed by studying the heterogeneous oxidation of simple, chemically tractable model systems. The surrogate organics used in this study, chosen for their high oxidation states and low vapor pressures, are citric acid ($C_6H_8O_7$; Aldrich, >99.5%), L-(+)-tartaric acid ($C_4H_6O_6$; Aldrich, >99.5%), and 1,2,3,4-butanetetracarboxylic acid (BTA, $C_8H_{10}O_8$; Aldrich, 99%). Molecular structures and the average carbon oxidation state ($\overline{OS_C}$)[5] of these model compounds and the three compounds from our previous studies[10,12] are provided in Figure 1. Additionally, the aging of a more complex organic mixture, Suwannee River fulvic acid (SRFA, obtained from IHSS), is also examined. SRFA has an $\overline{OS_C}$ that lies between 0.2 and 0.3[17] and is commonly used as a surrogate for highly oxidized organic aerosol.[18,19]

Heterogeneous oxidation experiments are carried out in the same flow reactor used in our prior studies, which enables us to combine high OH concentrations and low residence times to quickly simulate multiple weeks of oxidation under ambient conditions. The reactor has been described in detail previously[10−12] and is discussed only briefly here. The reactor is made up of type-219 quartz, with a length of 130 cm, inner diameter of 2.5 cm, and residence time of ∼37s. Carrier flow consists of 5% O_2 in N_2 at 30% relative humidity. Particles are generated by atomizing and subsequently drying aqueous solutions of each of the starting compounds; the resulting particles, which have surface-weighted mean diameters of ∼130−145 nm, are drawn into the flow reactor at loadings of ∼500−650 $\mu g\ m^{-3}$. These loadings are sufficiently high to ensure that at equilibrium well over 99% of the starting compound is present in the condensed phase, so that even for the most volatile compounds, gas-phase reactions will account for a very small fraction (<5%) of the total oxidation, assuming typical rates of hydrogen abstraction by OH.[20]

Ozone is produced by either a mercury pen-ray lamp or a commercial corona discharge ozone generator (OzoneLab Instruments). O_3 concentrations, which control the level of OH exposure within the reactor, are measured using an ozone monitor (2B Technologies Inc.). Within the flow reactor (temperature: 35 °C), ozone is photolyzed by UV light at 254 nm from two mercury lamps positioned immediately outside the quartz tube. $O(^1D)$ generated by ozone photolysis reacts with water vapor to form a pair of hydroxyl radicals (OH), which initiate oxidation of the particles. The relative humidity in the flow tube, maintained at 30%, is sufficiently high to ensure that direct oxidation of organics by $O(^1D)$ is negligible, as determined previously,[7] but also small enough to inhibit hygroscopic growth (∼5% for organic acids) and the subsequent formation of an aqueous phase.[18,21−23] Hexane (∼100 ppb) added to the tube is monitored by GC-FID to quantify OH concentration. This technique has been used to correctly predict rate constants in the reaction of OH with other selected gas-phase organics;[10,11] OH concentrations, which are changed by varying O_3, range from $\sim 1 \times 10^9$ to 3×10^{11} molecules cm^{-3}. These concentrations correspond to atmospheric OH exposures of approximately one day to four weeks, assuming an average ambient OH concentration of 3×10^6 molecules cm^{-3}.

Particles exiting the flow reactor are sampled into a scanning mobility particle sizer (SMPS, TSI, Inc.), for the measurement of particle mobility diameters, and a high-resolution time-of-flight aerosol mass spectrometer (HR-ToF-AMS, Aerodyne Research, Inc.), for the measurement of particle composition and vacuum aerodynamic diameter. Particle mass is determined by multiplying the average particle volume (from the SMPS) by the effective particle density, which is in turn calculated from the ratio of the vacuum aerodynamic diameter (obtained from the AMS) to the mobility diameter (obtained from the SMPS).[24] Although this method is strictly valid only for spherical particles, minor variations in particle shape will result

dx.doi.org/10.1021/jp212131m | J. Phys. Chem. A 2012, 116, 6358−6365

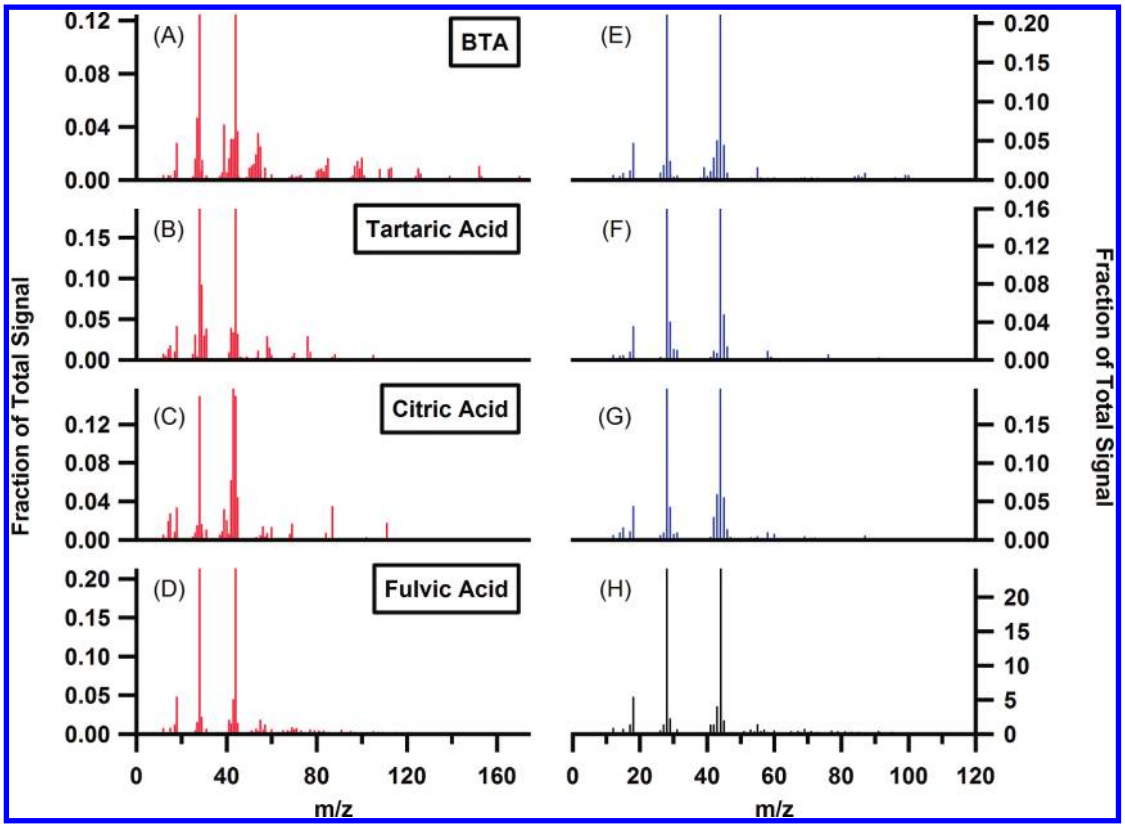

Figure 2. Aerosol mass spectra of reactants and products. (A–D) Mass spectra of unoxidized BTA, citric acid, tartaric acid, and fulvic acid, respectively. The spectra of the single-component systems (panels A–C) contain several high-mass ion fragments, which are used to identify the relative amount of the starting compound left in the mixture at a given level of oxidation. (E–G) Product mass spectra of the oxidation of BTA, citric acid, and tartaric acid, respectively, determined by spectral subtraction of the unoxidized spectra from the most oxidized spectra. (H) Mass spectrum of oxidized fulvic acid at the highest OH exposure. Residual spectra, and the mass spectrum of unoxidized fulvic acid, are dominated by low-mass oxygenated ion fragments, consistent with ambient measurements of oxidized organic aerosol.[1].

in only small errors (<10%) in measured mass.[24] Measured effective densities do not vary significantly during the course of the experiments.

Particles of pure components do not change in composition or mass when the UV lights were turned on with no ozone added, verifying both that the parent organic compounds studied are not directly photolyzed and that UV-generation of condensed-phase oxidants is negligible. Likewise, there are no compositional changes observed in the presence of ozone and absence of light, suggesting that direct reaction of the particles with ozone is negligible. Significant gas-phase oxidation of the compounds studied here is also highly unlikely, due to the strong partitioning into the particle phase and to the short residence time in the flow reactor.

We characterize the chemical changes to the reacting systems in terms of changes to the overall elemental composition of organics in the condensed phase. In particular, the oxygen-to-carbon ratio (O/C) and hydrogen-to-carbon ratio (H/C) are combined to estimate the overall degree of oxidation of the organic particles and the relative contributions of key functional groups. The method for calculating elemental ratios from high-resolution AMS data is described in detail by Aiken et al.[25,26]

RESULTS AND DISCUSSION

Sample mass spectra of the model systems are presented in Figure 2. In all cases, the chemical composition of the aerosol was observed to change dramatically with OH exposure.

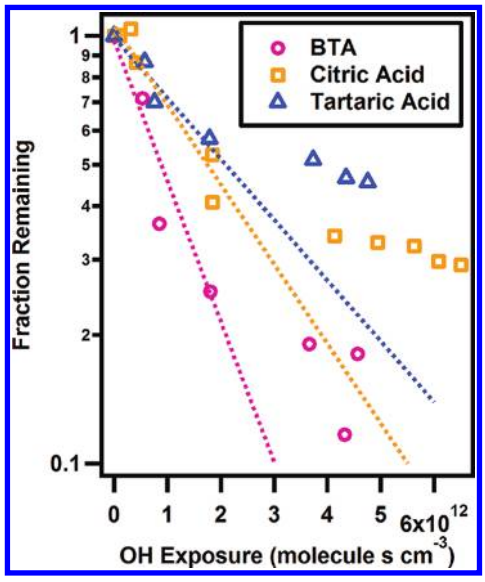

Figure 3. Mass fraction remaining of marker ions in the oxidation of the single-component systems. $C_8H_8O_3^+$ (m/z = 152) is used for BTA, $C_4H_4O^+$ (m/z = 68) for citric acid, and $C_4H_2O_3^+$ (m/z = 98) for tartaric acid. An exponential fit to the initial decay, at exposures up to 2 × 10^{12} molecule s cm^{-3}, is used to estimate the effective second-order rate coefficient for reaction with OH. The fitted trace is displayed over the data.

dx.doi.org/10.1021/jp212131m | J. Phys. Chem. A 2012, 116, 6358–6365

Table 1. Uptake Coefficients, Atmospheric Lifetime, and Van Krevelen Slope of Model Systems[a]

	BTA	Citric Acid	Tartaric Acid	Fulvic Acid
k (cm^3 $molecule^{-1}$ s^{-1})	$(7.6 \pm 2.4) \times 10^{-13}$	$(4.3 \pm 0.8) \times 10^{-13}$	$(3.3 \pm 0.9) \times 10^{-13}$	N.D.
$\gamma_{i,OH}$	0.51 ± 0.19	0.37 ± 0.08	0.40 ± 0.13	N.D.
atmospheric lifetime (days)[b]	8	13	17	N.D.
Van Krevelen slope	-0.31 ± 0.02	-0.33 ± 0.01	-0.60 ± 0.02	-0.59 ± 0.05

[a]All error bars reflect the 95% confidence intervals. [b]Assuming particles with a diameter of 200 nm, at an average OH concentration of 3×10^6 molecules cm^{-3}.

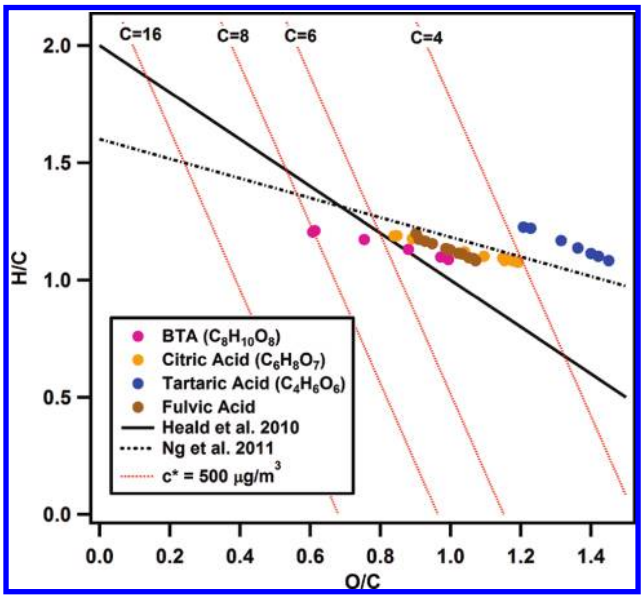

Figure 4. Van Krevelen diagram showing the elemental hydrogen-to-carbon (H/C) ratio vs oxygen-to-carbon (O/C) at all points during the oxidation of the four systems in this study. The solid black line represents observations of ambient aerosol at moderate levels of oxidation.[33] The dashed black line represents measurements of ambient organic aerosol at higher oxidation levels.[34] Red contours represent lines of constant volatility—the approximate number of carbon atoms a molecule must have at a given elemental composition to maintain a saturation concentration of 500 μg m^{-3}. As compounds become more oxidized, a shallower slope leads them more quickly to a region that allows a lower carbon content for the same volatility (or, conversely, lowers the volatility for a fixed number of carbon atoms).

i. Oxidation Kinetics. The rate of heterogeneous oxidation is quantified by measuring the decay of the parent compound, as estimated by a selected marker ion. The marker ion selected for each experiment is identified by spectral subtraction. The mass spectrum of the pure component in each system is scaled and subtracted from the average spectrum at every subsequent oxidant exposure level, so that the resulting residual spectrum contains no negative peaks beyond a specified tolerance (peaks contributing less than 0.1% of the total mass are ignored to avoid confounding effects of a small background signal). The ion that most frequently disappears first in each system is chosen as the marker ion: $C_4H_2O_3^+$ ($m/z = 98$) for tartaric acid, $C_4H_4O^+$ ($m/z = 68$) for citric acid, and $C_8H_8O_3^+$ ($m/z = 152$) for BTA. Mass spectra of the three single-component systems and residual spectra from the highest level of oxidation are provided in Figure 2. In all cases, the residual spectra—which represent oxidation products—are dominated by low-mass fragment ions such as m/z 44 (CO_2^+) and so do not provide suitable marker ions for the study of subsequent generations of oxidation. The mass spectrum of unoxidized fulvic acid is also shown in Figure 2; because it does not exhibit any sufficiently distinct marker ions, its kinetic behavior could not be determined.

The intensity of the selected marker ions are plotted in Figure 3 against OH exposure. Second-order rate constants for the reaction of the particulate organic species with OH are estimated from an exponential fit, using only values corresponding to OH exposures below 2×10^{12} molecule s cm^{-3}, the range over which the parent organic species decays exponentially (in this study and in our previous work[11,12]). The leveling-off observed for the marker ions at high OH exposures may be a result of a mass transfer limitation, possibly caused by changes in phase or viscosity,[27,28] or of the saturation of available adsorption sites on the particles.[9,29] Such effects may prevent the oxidation of all of the parent species over the short time scale (~37s) and high oxidant concentrations of the experiment. This approach also assumes that the level of oxidation in the reactor varies only as the product of average OH concentration times the residence time. Secondary processes that do not vary linearly with the amount of oxidant present are more likely to have a strong effect at very high concentrations.[7,29] Rate constants, determined for each single-component aerosol type, are listed in Table 1.

From the second-order rate coefficients and other known parameters of the system, we also calculate the effective reactive uptake coefficient, defined as the ratio of the initial rate of reactive loss of the parent species to the OH collision rate with the particle surface.[11] The uptake coefficient is calculated from the rate constant according to

$$\gamma_{i,OH} = \frac{2D_0\rho_i N_A}{3\bar{c}_{OH}M_i}\chi(D_0)k_{i,OH} \quad (1)$$

where D_0 is the surface-area-weighted mean particle diameter of unreacted particles, ρ_i is the component density, M_i is the component molecular weight, N_A is Avogadro's number, $\bar{c}_{OH}$ is the mean speed of hydroxyl radicals, and $\chi(D_0)$ is the diffusion correction factor.[30] Application of this diffusion correction accounts for a 15−30% increase in the calculated uptake coefficients. Equation 1 is valid when particulate species remain well-mixed on the time scales of the chemical reaction, so that all components are exposed to oxidants approximately equally. The changing concentrations shown in Figure 3, which initially decay exponentially but then level off, suggest that this is a good assumption at low OH exposures but possibly not after substantial oxidation.

Uptake coefficients determined for the three single-component systems are listed in Table 1, with values ranging from 0.37 to 0.51. These values are of the same order of magnitude as our previous measurements of coefficients for squalane (0.29),[11] erythritol (0.77), and levoglucosan (0.91).[12] For those compounds, heterogeneous reaction is expected to be fast, due to the large number of hydrogen atoms available for abstraction by OH. However, the highly oxidized species studied here also exhibit similarly high reaction probabilities,

dx.doi.org/10.1021/jp212131m | J. Phys. Chem. A 2012, 116, 6358−6365

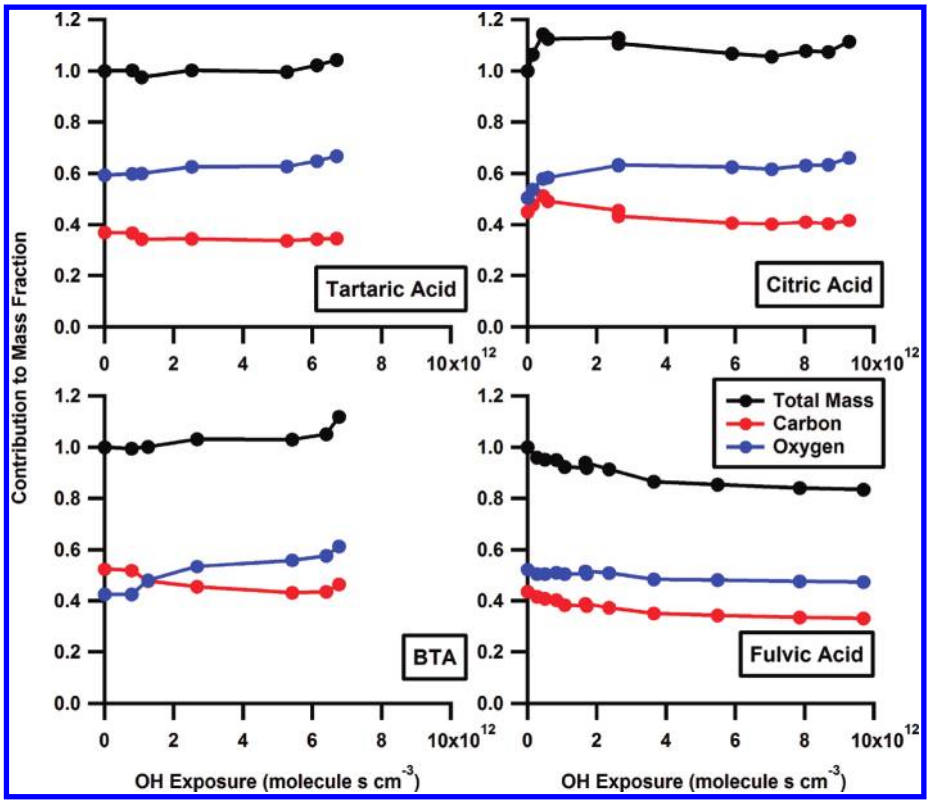

Figure 5. Fractional mass contribution of carbon (red) and oxygen (blue), and total mass fraction remaining per particle (black) for each of the four systems over the course of oxidation. The *x*-axis in each plot is an effective OH exposure, adjusting to a mean particle diameter of 200 nm in each system. Total mass in each pure component system remains unchanged, as the loss of carbon is offset by an approximately equivalent increase in oxygen.

despite having relatively few hydrogen atoms. This suggests that reactive uptake may be aided by the adsorption of OH to the particle surface prior to reaction, giving the radical more time to find a hydrogen atom available for abstraction before diffusing away from the particle.[9] This proposed effect is consistent with work by Vlasenko et al., which found that heterogeneous H-atom abstraction is a selective process despite high reaction probabilities.[31]

These large uptake coefficients suggest that heterogeneous oxidation will occur on atmospherically relevant time scales. Indeed, the lifetime against reaction with OH, estimated for particles with a diameter of 200 nm and an average OH concentration of 3×10^6 molecules cm^{-3}, ranges from 8 to 17 days (Table 1), as compared with a depositional lifetime of ~10 days for similarly sized particles.[32]

ii. Elemental Analysis. A van Krevelen plot in Figure 4 shows the oxidation trajectories of each of the four systems studied in terms of the hydrogen-to-carbon (H/C) and oxygen-to-carbon (O/C) ratios. To compare the results with similar studies of ambient organic aerosol,[33,34] we calculate elemental ratios using the approach and empirical correction factor proposed by Aiken et al.[25,26] The measured H/C and O/C values of the pure compounds tend to be lower than their exact values—an effect that has been previously reported for pure compounds using this technique.[25] However, the overall trends observed in the trajectories remain unchanged, regardless of the correction factor used. The slope of the trajectory is indicative of the average chemical transformation of particulate organics.[33] For example, a slope of 0 corresponds to the addition of hydroxyl groups (oxygen addition with no net hydrogen loss), −2 corresponds to carbonyl addition, and steeper slopes denote the conversion of functional groups (e.g., hydroxyl to carbonyl, which involves a loss of hydrogen with no oxygen addition). On the other hand, if the oxidation reaction involves fragmentation—the cleavage of C−C bonds—and subsequent loss of carbon to the gas phase, then the resulting slope can take on a range of different values, depending on the chemical characteristics of the volatilized fragment. Though previous studies have observed that measured ratios and trajectories of reduced and lightly oxidized organic aerosol follow a line with a slope of −1,[33] the data presented here have slopes ranging from −0.6 to −0.3 (Table 1). This tendency of more highly oxidized systems to acquire oxygen with a smaller net loss of hydrogen is consistent with recent studies of the aging of oxidized organic aerosol.[34]

One possible reason for the shift in slopes may be that at higher oxidation levels, reactions leading only to oxygen addition, such as the formation of hydroxyl groups, are more strongly favored.[34] However, the volatility of oxidation products likely also plays an important role, because the elemental ratios describe only those organics of sufficiently low volatility to be present in the particle phase. This effect is illustrated in Figure 4, which relates elemental ratios (position in van Krevelen space), vapor pressure, and carbon number. The contours define the carbon number required for an organic compound to be present (at least 50%) in the particle phase under the conditions of the present experiments (i.e., where saturation vapor concentration equals aerosol loading,[35,36] ~500 $\mu g\ m^{-3}$). These contours were determined by relating each point in van Krevelen space to a functional group distribution, assuming only hydroxyl, carbonyl, and carboxylic acid functionalities and estimating vapor pressures for a given number of carbon atoms

dx.doi.org/10.1021/jp212131m | J. Phys. Chem. A 2012, 116, 6358−6365

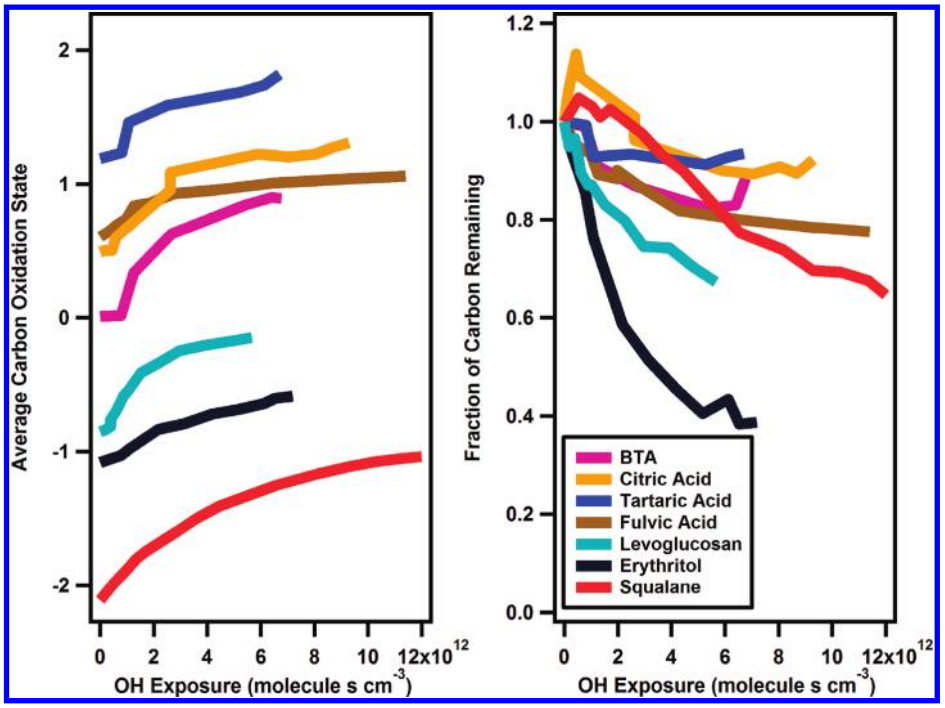

Figure 6. Summary of heterogeneous oxidation experiments. (A) Average carbon oxidation state as estimated from AMS elemental analysis[25,26] during the course of oxidation of squalane,[10] erythritol,[12] levoglucosan,[12] and the systems examined in this work. In all cases OH exposure is adjusted for a particle diameter of 200 nm (as in Figure 4). In general, there is an initial increase in oxidation state, at approximately the same rate, regardless of the system studied. (B) Estimated carbon loss, which serves as a measure of volatilization, for the same seven systems. Squalane, a reduced compound, undergoes moderate carbon loss. The moderately oxidized species, erythritol and levoglucosan, lose a much larger proportion of initial carbon to the gas phase, probably due to increased fragmentation reactions. On the other hand, the most oxidized species (the acids examined in the present study) experience only mild volatilization, possibly because fragmentation products are so low in volatility that they remain in the condensed phase.

using the SIMPOL group additivity method.[37] Organic species with high O/C and H/C values (the upper-right quadrant of the van Krevelen plot) are low in volatility and can therefore have a low carbon number while remaining in the condensed phase. Therefore, as oxidation proceeds, and as fragmentation (C−C cleavage) reactions become increasingly important,[10,38] particulate products are most likely to be found in this area of van Krevelen space. This effect may explain the shallower slopes associated with the oxidation of highly oxidized species.

The detailed reactions involved in the heterogeneous oxidation processes studied here are not well-understood, because the oxidation mechanisms of highly oxidized species have not received nearly as much attention as those of reduced organic species.[38] However, we can gain insight into general features of this chemistry (e.g., functionalization vs fragmentation of the carbon skeleton) from the changes in particle mass and elemental abundances. Figure 5 shows the particulate mass fraction remaining and the relative abundances of carbon and oxygen atoms in each of the systems studied, plotted against OH exposure. The exposure levels are adjusted to account for differences in particle size among experiments; the values presented are the estimated equivalent exposures for a particle with a surface-area-weighted mean diameter of 200 nm, using the relationship between rate coefficient and diameter presented in eq 1. The slight increase in mass for the BTA and citric acid systems at the highest OH exposure level is attributed to fluctuation in the atomizer output, which causes the particle distribution to shift to larger diameters, rather than to a physical or chemical effect within the reactor. For each of the three pure-component systems, the loss of carbon by volatilization processes—principally fragmentation during oxidation—is offset by the addition of oxygen atoms, so that the total particle mass remains approximately constant. As a result, the primary effect of heterogeneous oxidation is to change particle composition (and therefore physicochemical properties), but not total mass. Although there might be a mass transfer barrier that could prevent us from observing some eventual mass loss,[39] our previous studies on more reduced systems have demonstrated our capability for observing more significant mass changes on similar time scales.[12] Moreover, our observation that the particles do not experience a significant change in mass upon aging is consistent with results from recent field measurements, which find that particle O/C, but not mass, increases with photochemical age.[40−42]

■ CONCLUSIONS

Summary plots of key changes to particles upon heterogeneous oxidation are provided in Figure 6 for all of the systems studied here, as well as those from our previous work (squalane, erythritol, and levoglucosan).[10,12] Figure 6a shows the overall degree of oxidation of the condensed-phase organics, as described by the average carbon oxidation state, approximated by the equation $\overline{OS}_C \approx 2(O/C) - H/C$[5]. Regardless of the initial system chosen, there is invariably a marked increase in the level of oxidation upon exposure to OH. Furthermore, analysis of the atmospheric lifetimes of these compounds indicates that such chemical transformation by heterogeneous oxidation occurs on time scales commensurate with particle loss by deposition.[32] This is of particular significance for the lowest-volatility fraction of the oxidized organic aerosol, which is

dx.doi.org/10.1021/jp212131m | J. Phys. Chem. A 2012, 116, 6358−6365

unlikely to be found in the gas phase and thus must undergo oxidation in the condensed phase—either by heterogeneous reaction with OH or via aqueous-phase chemistry.[43]

Additionally, Figure 6b shows the relative carbon content of each system as a function of OH exposure. Carbon loss serves as a useful proxy for volatilization of the particulate organic species; all systems exhibit some carbon loss, indicating that heterogeneous oxidation leads to the formation of oxidized species not only in the particle phase but also in the gas phase. Although the degree of carbon loss varies from species to species, likely due to differences in carbon number and molecular structure, general trends with oxidation state are apparent. The least oxidized species (squalane, a saturated alkane) initially does not undergo any volatilization upon oxidation, due to the dominance of functionalization over fragmentation reactions.[5] As it gets more oxidized, however, further oxidation leads to significant loss of carbon (and total particle mass). This trend is also seen for the moderately oxidized species, erythritol and levoglucosan, which exhibit the most rapid volatilization. However, for the most oxidized species (the polycarboxylic acids examined in this work), carbon loss is restricted over the course of the experiment to no more than ~20%. This may be because fragmentation processes which otherwise contribute strongly to volatilization[10] either are less favored during oxidation or, more likely, produce fragments that are sufficiently low in volatility that they remain in the condensed phase. Furthermore, the loss of carbon for the most oxidized species is typically offset by an equivalent increase in oxygen, so that the overall process approximately conserves particle mass. Atmospheric oxidation of the most oxidized organic aerosol is therefore unlikely to be a significant sink of aerosol mass, though it is still capable of transforming the chemical composition—and therefore key properties such as hygroscopicity[1,9,44−46] and refractive index[44]—of the particles over their atmospheric lifetimes.

AUTHOR INFORMATION

Corresponding Author

*E-mail: jhkroll@mit.edu.

Notes

The authors declare no competing financial interest.

ACKNOWLEDGMENTS

This work was supported by the National Science Foundation (Grants No. CHE-1012809 and AGS-1056225) and the Director, Office of Energy Research, Office of Basic Energy Sciences, Chemical Sciences Division of the U.S. Department of Energy under Contract No. DE-AC02-05CH11231. J.D.S. was supported by the Camille and Henry Dreyfus foundation postdoctoral program in environmental chemistry.

REFERENCES

(1) Jimenez, J. L.; Canagaratna, M. R.; Donahue, N. M.; Prevot, A. S. H.; Zhang, Q.; Kroll, J. H.; DeCarlo, P. F.; Allan, J. D.; Coe, H.; Ng, N. L.; et al. *Science* **2009**, *326*, 1525.

(2) George, I. J.; Vlasenko, A.; Slowik, J. G.; Broekhuizen, K.; Abbatt, J. P. D. *Atmos. Chem. Phys.* **2007**, *7*, 4187−4201.

(3) Lambe, A. T.; Ahern, A. T.; Williams, L. R.; Slowik, J. G.; Wong, J. P. S.; Abbatt, J. P. D.; Brune, W. H.; Ng, N. L.; Wright, J. P.; Croasdale, D. R.; Worsnop, D. R.; Davidovits, P.; Onasch, T. B. *Atmos. Meas. Tech.* **2011**, *4*, 445−461.

(4) Lambe, A. T.; Onasch, T. B.; Massoli, P.; Croasdale, D. R.; Wright, J. P.; Ahern, A. T.; Williams, L. R.; Worsnop, D. R.; Brune, W. H.; Davidovits, P. *Atmos. Chem. Phys.* **2011**, *11*, 8913−8928.

(5) Kroll, J. H.; Donahue, N. M.; Jimenez, J. L.; Kessler, S. H.; Canagaratna, M. R.; Wilson, K. R.; Altieri, K. E.; Mazzoleni, L. R.; Wozniak, A. S.; Bluhm, H.; et al. *Nat. Chem.* **2011**, *3*, 133−139.

(6) Hearn, J. D.; Renbaum, L. H.; Wang, X; Smith, G. D. *Phys. Chem. Chem. Phys.* **2007**, *9*, 4803−4813.

(7) McNeill, V. F.; Yatavelli, R. L. N.; Thornton, J. A.; Stipe, C. B.; Landgrebe, O. *Atmos. Chem. Phys.* **2008**, *8*, 5465−5476.

(8) George, I. J.; Abbatt, J. P. D *Atmos. Chem. Phys.* **2010**, *10*, 5551−5563.

(9) George, I. J.; Abbatt, J. P. D *Nat. Chem.* **2010**, *2*, 713−722.

(10) Kroll, J. H.; Smith, J. D.; Che, D. L.; Kessler, S. H.; Worsnop, D. R.; Wilson, K. R. *Phys. Chem. Chem. Phys.* **2009**, *11*, 8005−8014.4.

(11) Smith, J. D.; Kroll, J. H.; Cappa, C. D.; Che, D. L.; Liu, C. L.; Ahmed, M.; Leone, S. R.; Worsnop, D. R.; Wilson, K. R. *Atmos. Chem. Phys.* **2009**, *9*, 3209−3222.

(12) Kessler, S. H.; Smith, J. D.; Che, D. L.; Worsnop, D. R.; Wilson, K. R.; Kroll, J. H. *Environ. Sci. Technol.* **2010**, *44*, 7005−7010.

(13) Rudich, Y.; Donahue, N. M.; Mentel, T. F. *Annu. Rev. Phys. Chem.* **2007**, *58*, 321−352.

(14) Cappa, C. D.; Jimenez, J. L. *Atmos. Chem. Phys.* **2010**, *10*, 5409−5424.

(15) Huffman, J. A.; Docherty, K. S.; Aiken, A. C.; Cubison, M. J.; Ulbrich, I. M.; DeCarlo, P. F.; Sueper, D.; Jayne, J. T.; Worsnop, D. R.; Ziemann, P. J.; Jimenez, J. L. *Atmos. Chem. Phys.* **2009**, *9*, 7161−7182.

(16) Huffman, J. A.; Docherty, K. S.; Mohr, C.; Cubison, M. J.; Ulbrich, I. M.; Ziemann, P. J.; Onasch, T. B.; Jimenez, J. L. *Environ. Sci. Technol.* **2009**, *43*, 5351−5357.

(17) IHSS - Elemental Compositions and Stable Isotopic Ratios of IHSS Samples http://www.humicsubstances.org/elements.html (accessed Mar 5, 2012).

(18) Su, H.; Rose, D.; Cheng, Y. F.; Gunthe, S. S.; Massling, A.; Stock, M.; Wiedensohler, A.; Andreae, M. O.; Pöschl, U. *Atmos. Chem. Phys.* **2010**, *10*, 7489−7503.

(19) Fuzzi, S.; Decesari, S.; Facchini, M. C.; Matta, E.; Mircea, M.; Tagliavini, E. *Geophys. Res. Lett.* **2001**, *28*, 4079−4082.

(20) Atkinson, R.; Baulch, D. L.; Cox, R. A.; Hampson, R. F.; Kerr, J. A.; Rossi, M. J.; Troe, J. *J. Phys. Chem. Ref. Data* **1999**, *28*, 191.

(21) Peng, C.; Chan, M. N.; Chan, C. K. *Environ. Sci. Technol.* **2001**, *35*, 4495−4501.

(22) Choi, M. Y.; Chan, C. K. *Environ. Sci. Technol.* **2002**, *36*, 2422−2428.

(23) Cruz, C. N.; Pandis, S. N. *Environ. Sci. Technol.* **2000**, *34*, 4313−4319.

(24) DeCarlo, P.; Slowik, J. G.; Worsnop, D. R.; Davidovits, P.; Jimenez, J. L. *Aero. Sci. Technol.* **2004**, *38*, 1185−1205.

(25) Aiken, A. C.; DeCarlo, P. F.; Jimenez, J. L. *Anal. Chem.* **2007**, *79*, 8350−8358.

(26) Aiken, A. C.; DeCarlo, P. F.; Kroll, J. H.; Worsnop, D. R.; Huffman, J. A.; Docherty, K. S.; Ulbrich, I. M.; Mohr, C.; Kimmel, J. R.; Sueper, D.; et al. *Environ. Sci. Technol.* **2008**, *42*, 4478−4485.

(27) Hearn, J. D.; Smith, G. D. *Phys. Chem. Chem. Phys.* **2005**, *7*, 2549−2551.

(28) Renbaum, L. H.; Smith, G. D. *Phys. Chem. Chem. Phys.* **2009**, *11*, 2441−2451.

(29) Renbaum, L. H.; Smith, G. D. *Atmos. Chem. Phys.* **2011**, *11*, 6881−6893.

(30) Fuchs, N. A.; Sutugin, A. G. *Highly dispersed aerosols*; Halsted Press: New York, 1970.

(31) Vlasenko, A.; George, I. J.; Abbatt, J. P. D *J. Phys. Chem. A* **2008**, *112*, 1552−1560.

(32) Balkanski, Y. J.; Jacob, D. J.; Gardner, G. M.; Graustein, W. C.; Turekian, K. K. *J. Geophys. Res.* **1993**, *98*, 20573−20586.

(33) Heald, C. L.; Kroll, J. H.; Jimenez, J. L.; Docherty, K. S.; DeCarlo, P. F.; Aiken, A. C.; Chen, Q.; Martin, S. T.; Farmer, D. K.; Artaxo, P. *Geophys. Res. Lett.* **2010**, *37*, L08803.

(34) Ng, N. L.; Canagaratna, M. R.; Jimenez, J. L.; Chhabra, P. S.; Seinfeld, J. H.; Worsnop, D. R. *Atmos. Chem. Phys.* **2011**, *11*, 6465−6474.
(35) Donahue, N. M.; Robinson, A. L.; Stanier, C. O.; Pandis, S. N. *Environ. Sci. Technol.* **2006**, *40*, 2635−2643.
(36) Odum, J. R.; Hoffmann, T.; Bowman, F.; Collins, D.; Flagan, R. C.; Seinfeld, J. H. *Environ. Sci. Technol.* **1996**, *30*, 2580−2585.
(37) Pankow, J. F.; Asher, W. E. *Atmos. Chem. Phys.* **2008**, *8*, 2773−2796.
(38) Atkinson, R. *Atmos. Environ.* **2000**, *34*, 2063−2101.
(39) Virtanen, A.; Joutsensaari, J.; Koop, T.; Kannosto, J.; Yli-Pirilä, P.; Leskinen, J.; Mäkelä, J. M.; Holopainen, J. K.; Pöschl, U.; Kulmala, M.; et al. *Nature* **2010**, *467*, 824−827.
(40) Dunlea, E. J.; DeCarlo, P. F.; Aiken, A. C.; Kimmel, J. R.; Peltier, R. E.; Weber, R. J.; Tomlinson, J.; Collins, D. R.; Shinozuka, Y.; McNaughton, C. S.; et al. *Atmos. Chem. Phys.* **2009**, *9*, 7257−7287.
(41) Capes, G.; Johnson, B.; McFiggans, G.; Williams, P. I.; Haywood, J.; Coe, H. *J. Geophys. Res.* **2008**, *113*, D00C15.
(42) DeCarlo, P. F.; Dunlea, E. J.; Kimmel, J. R.; Aiken, A. C.; Sueper, D.; Crounse, J.; Wennberg, P. O.; Emmons, L.; Shinozuka, Y.; Clarke, A. *Atmos. Chem. Phys.* **2008**, *8*, 4027−4048.
(43) Ervens, B.; Turpin, B. J.; Weber, R. J. *Atmos. Chem. Phys.* **2011**, *11*, 11069−11102.
(44) Cappa, C. D.; Che, D. L.; Kessler, S. H.; Kroll, J. H.; Wilson, K. R. *J. Geophys. Res.* **2011**, *116*, D15204.
(45) Massoli, P.; Lambe, A. T.; Ahern, A. T.; Williams, L. R.; Ehn, M.; Mikkilä, J.; Canagaratna, M. R.; Brune, W. H.; Onasch, T. B.; Jayne, J. T. *Geophys. Res. Lett.* **2010**, *37*, L24801.
(46) Chang, R. Y.-W.; Slowik, J. G.; Shantz, N. C.; Vlasenko, A.; Liggio, J.; Sjostedt, S. J.; Leaitch, W. R.; Abbatt, J. P. D. *Atmos. Chem. Phys.* **2010**, *10*, 5047−5064.